Journal of Catalysis 335 (2016) 117–124

Contents lists available at ScienceDirect

Journal of Catalysis

journal homepage: www.elsevier.com/locate/jcat

# Determination of acid sites in porous aluminosilicate solid catalysts for aqueous phase reactions using potentiometric titration method

Kai Yu [a], Narendra Kumar [a], Atte Aho [a], Jorma Roine [b], Ivo Heinmaa [c], Dmitry Yu. Murzin [a], Ari Ivaska [a,*]

[a] Johan Gadolin Process Chemistry Centre, Åbo Akademi University, Biskopsgatan 8, 20500 Åbo/Turku, Finland
[b] Department of Physics and Astronomy, University of Turku, 20014 Åbo/Turku, Finland
[c] National Institute of Chemical Physics and Biophysics, Akadeemia tee 23, 12618 Tallinn, Estonia

ARTICLE INFO

*Article history:*
Received 22 September 2015
Accepted 14 December 2015
Available online 18 January 2016

*Keywords:*
Zeolites
Potentiometric acid–base titration
Gran method
FTIR-pyridine
XRD
ICP-OES
NMR

ABSTRACT

A potentiometric acid–base titration method was developed to characterize the acid–base properties of H-Beta-25, H-Beta-300, H-Ferrierite-20 and Si-MCM-48 zeolites in aqueous solutions. The method is based on linearization of the titration curve. The zeolite powders were dispersed in a sodium nitrate solution which was then titrated with a standard solution of sodium hydroxide. Various acid sites were found in the studied zeolites, and both the protonation constants and the concentrations of these acid sites were determined. The chemical composition (aluminum and silicon), distribution of the aluminum sites, crystallinity as well as the acidic properties of the titrated zeolites were compared with those of the pristine zeolites by using Inductively Coupled Plasma Optical Emission Spectrometer (ICP-OES), X-ray Diffraction (XRD), $^{27}$Al NMR spectroscopy and the commonly used gas phase Fourier Transform Infrared spectroscopy (FTIR) of pyridine adsorption method.



## 1. Introduction

Zeolites are commonly composed by a three dimensional network of $SiO_4^{4-}$ tetrahedral structure [1]. When a heteroatom with lower valency than Si, such as Al, B, Ga and Fe, is introduced to the framework, the formal charge on that tetrahedron changes from neutral to negative. This negative charge is then balanced either with a hydroxyl proton to form a strong Brønsted acid site (BAS) or with a metal cation to form a weak Lewis acid site (LAS) [2]. Due to the presence of the acid sites in the framework structure, the solid acid and metal modified zeolites are used as catalytic materials in several petro-chemicals and oil refinery processes, as well as in synthesis of fine and specialty chemicals [3,4]. Acidic and metal modified zeolite catalysts are also used in environmental applications such as exhaust gas purification from mobile and stationary sources, pretreatment of industrial and municipal waste water stream, agricultural soil contamination and nuclear waste treatment [5–8]. Since these acid sites play an important role in the catalytic and sorption properties of zeolites [9], better knowledge of them is important for successful industrial applications of zeolites as solid catalysts.

Numerous gas phase methods and techniques have been published to quantify and characterize the acidity of zeolites. One of the methods uses Fourier Transform Infrared spectroscopy (FTIR) of various probe molecules (ammonia, pyridine) adsorption to study the fundamental stretching vibrations of hydroxyl groups at varying temperatures to determine the Brønsted and Lewis acid sites [10,11]. Another commonly used method is the temperature-programmed desorption (TPD) technique to measure the reacted amount of a gaseous base (ammonia) with zeolites for characterizing the density and strength of the acid sites [12]. Both FTIR-pyridine and TPD-ammonia methods are performed in the gas phase at high temperature (100–450 °C). However, many catalytic reactions especially related to valorization of biomass are carried out in aqueous solutions at ambient or somewhat elevated temperature [13,14] and therefore the catalytic properties based on the acidity of the zeolites determined with FTIR-pyridine and TPD may not be relevant. Therefore a technique, which can be used to characterize the acidic properties of the zeolites in the aqueous phase, is necessary.

Acid–base titration of zeolites in non-aqueous solvents has been used earlier to study the acidity of zeolites. The method was introduced by Benesi in 1950s [15] and then modified by other researchers [16]. In that method the surface of zeolite was titrated with amine, i.e., *n*-butylamine, in a non-aqueous solvent and a series of Hammett indicators with various acidity constant values or $pK_a$ values, i.e., benzeneazodiphenylamine ($pK_a = 1.5$) and

* Corresponding author. Fax: +358 22154479.
*E-mail address:* ari.ivaska@abo.fi (A. Ivaska).

http://dx.doi.org/10.1016/j.jcat.2015.12.010
0021-9517/

phenylazonaphthylamine ($pK_a$ = 3.3), were used to characterize the acid sites [17]. However, it was demonstrated later that the additional indicators in the non-aqueous solvent could disturb the equilibrium state of the zeolite system during the titration [18,19]. Another drawback of using the Hammett indicators is their molecule size, which is too large for the indicator molecules to enter the channels and cages of some zeolites [20]. Due to these fundamental limitations and the long time of the experiments, the titration using indicators did not become a popular technique in studying zeolites.

In the current study, a specific potentiometric acid–base titration method developed from the traditional titration method will be used to characterize the acid sites in zeolites. This method has a high resolution in determining the various acid groups present in the samples. Moreover, it is not necessary to use any indicators to monitor the acid–base reaction. During the titration, pH of the solution is measured as a function of the volume of a strong base added and the obtained titration curve is used to analyze the titrated samples. In addition, the small $OH^-$ ions can penetrate deep inside the zeolite channels and the acid sites in those channels can therefore also be determined.

The studied zeolites are the proton forms of H-Beta type with $SiO_2/Al_2O_3$ ratios of 25 and 300, H-Ferrierite type with $SiO_2/Al_2O_3$ ratio of 20 and Si-MCM-48 which belongs to a pristine silica mesoporous material without any aluminum in the framework. The frameworks of Beta, Ferrierite and Si-MCM-48 are shown in Fig. 1 [21,22]. The three dimensional structure of the Beta zeolite has two tetragonal crystal systems: one channel consists of 12-membered rings with dimensions of 5.6 × 5.6 Å and the other consists of 12-membered ring with dimensions of 6.6 × 6.7 Å. The two dimensional structure of the Ferrierite zeolite contains two type channel systems: one channel consists of 8-membered rings with dimensions of 3.5 × 4.8 Å and the other consists of 10-membered rings with dimensions of 4.2 × 5.4 Å. The three dimensional cubic structure of Si-MCM-48 is composed by unconnected pore system with dimensions of 20–80 Å [22–24].

## 2. Experimental work

### 2.1. Chemicals

Two Beta type zeolites with $SiO_2/Al_2O_3$ ratios of 25 and 300 and one Ferrierite type zeolite with $SiO_2/Al_2O_3$ ratio of 20 were obtained in $NH_4$-form from Zeolyst International. $NH_4$-Beta-25, $NH_4$-Beta-300 and $NH_4$-Ferrierite-20 were calcined in a muffle oven at 450 °C for 4 h to generate H-Beta-25, H-Beta-300 and H-Ferrierite-20. A pristine silica mesoporous material Si-MCM-48 was prepared in our laboratory by using a modified templating hydro-thermal synthesis method described by Käldström et al. [25].

The titrant, 0.1 M NaOH + 0.1 M $NaNO_3$, was made from reagent-grade chemicals obtained from Merck and its accurate concentration was determined using the conventional acid–base standardization titration method. The titrant was stored in argon environment with carbon dioxide adsorbent to avoid $CO_2$ contamination. A stock solution of 0.1 M $NaNO_3$ was also prepared as the titration medium for the zeolites. The distilled water from system PureLAB Ultra (ELGA) was boiled to expel $CO_2$ before using it as the solvent for the NaOH and $NaNO_3$ solutions.

### 2.2. Potentiometric titration

Potentiometric titrations were performed with an automatic titration system Mettler Toledo DL 50 Graphix Titrator (Mettler Toledo GmbH Analytical). The pH was measured with a combined glass electrode DG111-SC from Mettler Toledo and the system was calibrated in standard buffer solutions of pH 4.00, 7.00 and 10.00 prior to use. A total of 10 ml titrant (NaOH) was consumed in the end of the titration. Titration of the zeolite suspension was performed only to pH 10 in order to avoid possible dissolution of the zeolites at higher pH values.

The Gran method, which is based on the Sørensen's [26] earlier work and described by Gran in 1952 [27], was selected for the data

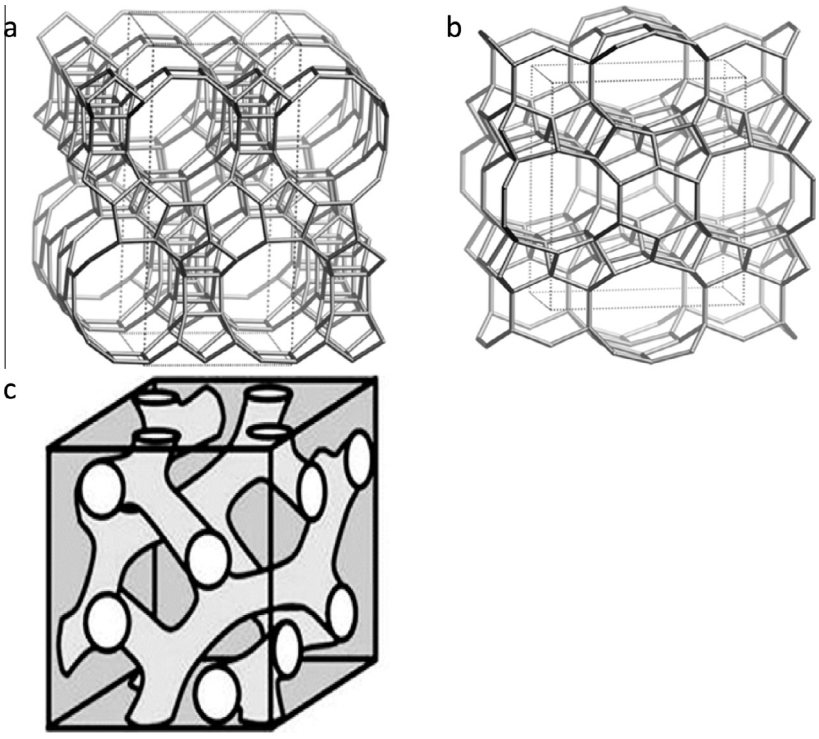


**Fig. 1.** Framework structure of zeolites, (a) Beta, (b) Ferrierite and (c) Si-MCM-48.

analysis in this work. The common sigmoidal potentiometric titration curve is transformed to a linear form with the Gran function, which allows calculation of the equivalence volume by a standard linear regression method using several points on the titration curve. The Gran functions used in this work and their derivations are shown in the supplement. Ingman and Still have derived a more accurate equation than (S14) to describe the titration of a weak acid with strong base [28]. Ivaska and Wänninen have developed that method further for simultaneous determination of both $V_{eq}$ and $K$ by an iterative computing method [29]. The Gran function can be used when the electrode system has a Nernstian response and that the activity coefficients of the species in the solution remain constant during the potentiometric titration.

The Gran functions are given in Table 1. A conventional titration curve, pH as function of $V$ (volume of added base), for titration of strong acid $HNO_3$ with strong base NaOH is shown in Fig. 2. When the same experimental data (pH vs. $V$) are processed with the Gran functions $f_1(V)$ and $f_2(V)$ the two straight lines in Fig. 2 are obtained. The numerical scales for $f_1(V)$ and $f_2(V)$ are different and not shown in the figure. The lines intersect each other on the $V$-axis at $V_{eq}$, which is known as the equivalence volume of the titration and can be used in calculating the concentration of $HNO_3$. Both lines can be used in determination of $V_{eq}$.

Because of the low concentration of the acid sites in zeolite, the suspension should be prepared within a high density of zeolite particles ($\geqslant$5.5 g/l), in order to obtain detectable and well-defined changes in the potentiometric titration curves. Accurately weighed zeolite samples, approximately 0.85 g, suspended in 150 ml of 0.1 M $NaNO_3$ solution were titrated by stepwise additions of the titrant under argon atmosphere. Prior to the titration, the zeolite suspension was purged with argon for 15 min to expel the dissolved $CO_2$ which otherwise would disturb the titration. The entire titration was performed in a closed beaker under argon atmosphere. Stirring the zeolite suspension is necessary in order to achieve an effective reaction between the acid sites and the strong base. The uniform concentration of $NaNO_3$ in the suspension and in the base solution keeps the ionic strength constant in both solutions, and ensures that the activity coefficients remain constant for all species during the experiments.

### 2.3. Characterization methods for pristine and titrated zeolites

The pristine and the titrated zeolites were both characterized in the study. The titrated zeolite samples were prepared by filtration of the suspension and dried at 50 °C for 24 h.

In order to determine the concentrations of the aluminum and silicon, which mainly contribute to the acid sites in the zeolites, the high resolution Inductively Coupled Plasma Optical Emission Spectrometer (ICP-OES) (Optima 5300DV, Perkin Elmer) was used. A certain amount of the zeolite powder (pristine or the titrated) was dissolved in a mixture of 4 ml HF (40%) + 1 ml $HNO_3$ (65%) + 1 ml HCl (30%) in a microwave oven and then the obtained solution was diluted to 100 ml to make the stock solution. 1 ml of the stock solution was diluted further to 100 ml, which was then analyzed by the ICP-OES technique.

$^{27}$Al MAS NMR spectra of the pristine and titrated zeolites were recorded on Bruker AVANCE III-800 spectrometer using a resonance frequency of 208.4 MHz. The spinning speed of the studied samples in all experiments was 23.0 kHz.

Crystallinity of the pristine zeolites as well as the titrated zeolites was characterized with X-ray diffraction using the Philips X'Pert Pro MPD X-ray powder diffractometer equipped with a Philips PW 3050/60 goniometer. The diffractometer was operated in Bragg–Brentano diffraction mode (for $2\theta$ angle ranging from 5.0° to 30.0°), and the monochromatized Cu $K\alpha$ radiation was generated with a voltage of 40 kV and a current of 50 mA.

Fourier Transform Infrared Spectroscopy (FTIR) (ATI Mattson) with pyridine as a probe molecule was used to measure the concentration of Brønsted and Lewis acid sites in the pristine and the titrated zeolites.

**Table 1**
Gran functions used in the potentiometric titration data analysis from the Supplement. $V_0$ is the volume of the sample solution, $V$ is the volume of titrant added, $C_{OH}$ is the concentration of the titrant and $K$ is the protonation constant of the acid.

| Substance titrated | Gran functions | |
|---|---|---|
| | On the acid side of the equivalence point | On the alkaline side of the equivalence point |
| Strong acid | $f_1(V) = \frac{(V_0+V)}{C_{OH}} \cdot 10^{-pH}$ | $f_2(V) = \frac{(V_0+V)}{C_{OH}} \cdot 10^{(pH-14)}$ |
| Weak acid | $f_3(V) = K \cdot 10^{-pH} \cdot V$ | $f_2(V) = \frac{(V_0+V)}{C_{OH}} \cdot 10^{(pH-14)}$ |

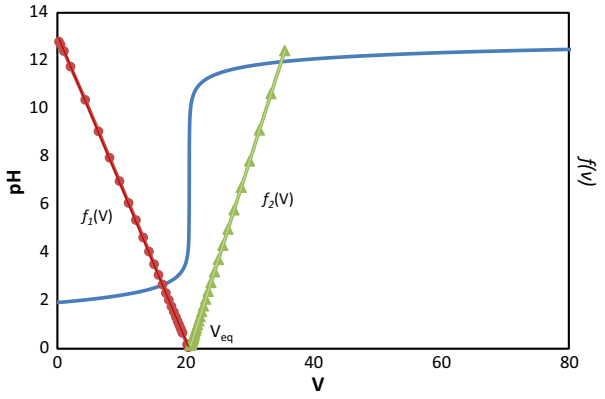


**Fig. 2.** Titration of 4 ml of 0.5 M $HNO_3$ with 0.1 M NaOH. The ▬ line is pH vs. $V$, i.e. the volume of added base. The linear Gran curves obtained with $f_1(V)$ and $f_2(V)$ have the same intersecting point on the $V$-axis and the point is the equivalence volume ($V_{eq}$). The markers on curves $f_1(V)$ and $f_2(V)$ show the positioning of the data points used for evaluating the $V_{eq}$. The numerical scale for the functions $f_1(V)$ and $f_2(V)$ is not shown.

## 3. Results and discussion

### 3.1. Acid–base characterization of zeolites

The acid–base properties of the zeolites in aqueous solutions can best be described by considering that the material contains several different acid sites with different strengths, i.e., different protonation constants, according to the following equilibria and constants:

$$R_1^- H^+ \rightleftharpoons R_1^- + H^+; K_1 = \frac{[R_1^- H^+]}{[R_1^-][H^+]}$$
$$R_2^- H^+ \rightleftharpoons R_2^- + H^+; K_2 = \frac{[R_2^- H^+]}{[R_2^-][H^+]}$$
$$\cdots\cdots\cdots\cdots\cdots\cdots\cdots\cdots$$
$$R_n^- H^+ \rightleftharpoons R_n^- + H^+; K_n = \frac{[R_n^- H^+]}{[R_n^-][H^+]}$$

where $R$ denotes the anionic part of the acid site. It should be pointed out that the concentrations of the different $R$, i.e., acid sites, are also different.

Potentiometric titration curves (pH vs. $V$, volume of added NaOH) of zeolites H-Beta-25, H-Beta-300, H-Ferrierite-20 and Si-MCM-48 are shown in Fig. 3. From the shapes of these curves it can be seen that all the titrated zeolites are acidic and contain various acid sites in their frameworks.

In Table 2, the protonation constants and the concentrations of the acid sites in the four zeolites are given after evaluation of the

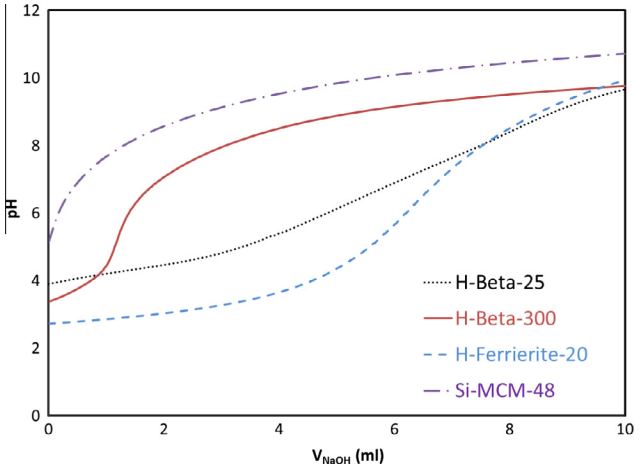


**Fig. 3.** Potentiometric titration curves of the pristine zeolites.

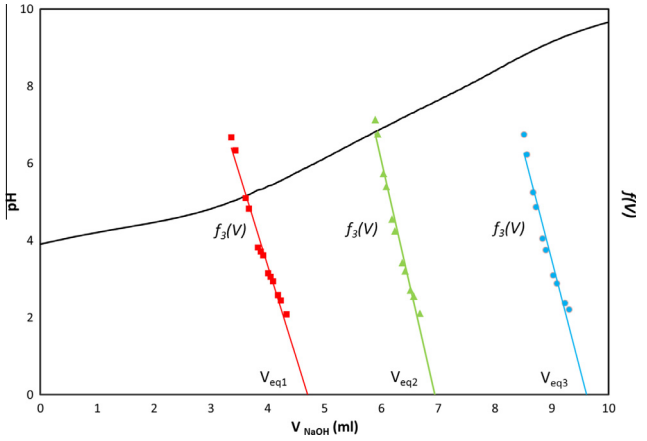


**Fig. 4.** Determination of the acid sites with the Gran method in titration of H-Beta-25. The points marked with ■, ▲ and ● are obtained by transforming the original titration data with the Gran function $f_3(V)$. The numerical scales for the different functions of $f_3(V)$ are not shown.

titration data with the Gran method. Due to the weak acidity of the zeolites, function $f_3(V)$ was used in this calculation. The method is explained in connection with Fig. 4. When the titration data of H-Beta-25 are processed with the function $f_3(V)$ (Table 1) some curvature with the first titration points was found. Only the points ■-■-■ lying on a straight line are shown in Fig. 4 and used in the calculations (see the explanation in the supplement). It should be pointed out that the numerical scales for the function $f_3(V)$ when calculating the three linear graphs are different and not shown in Fig. 4 for the sake of clarity. The intersection of the straight line with the $V$-axis gives $V_{eq1}$, i.e., the equivalence volume corresponding to the acid site $R_1^-H^+$, and that value is then used in calculating the concentration of $R_1^-H^+$. When the following points in the titration curve, pH vs. $V$, are evaluated in the similar way with the function $f_3(V)$ the next straight line ▲-▲-▲ is observed with $V_{eq2}$. The concentration of $R_2^-H^+$ can be calculated from $\Delta V_{eq2} = V_{eq2} - V_{eq1}$. The concentrations of $R_3^-H^+$ and $R_4^-H^+$ are also calculated in the same way. The protonation constants of these acid sites, i.e. $K_1$, $K_2$, $K_3$ and $K_4$ can simultaneously be obtained from the slope of the straight lines (see the supplement). The logarithmic values of $K_1$, $K_2$, $K_3$ and $K_4$ are also included in Table 2.

Depending on the lg $K$ values, these acid sites are separated into two categories: moderate acid sites and weak acid sites. The moderate acid sites, defined when its lg $K \leqslant 6.0$, are formed due to OH bridging a framework silicon to a framework aluminum. The weak acid sites, defined when its lg $K > 6.0$, are formed due to the fact that dehydroxylation of alumina hydrates into transition alumina generates coordinately unsaturated sites [30]. As can be seen in Table 2, both H-Beta-25 and H-Beta-300 contain one moderate acid site ($R_1^-H^+$) and two weak acid sites ($R_2^-H^+$ and $R_3^-H^+$) while H-Ferrierite-20 has two moderate acid sites ($R_1^-H^+$ and $R_2^-H^+$) and two weak acid sites ($R_3^-H^+$ and $R_4^-H^+$). Due to the absence of aluminum in Si-MCM-48, only one weak acid site ($R_3^-H^+$) was found in its framework. The strongest acid site is in H-Ferrierite-20 with the lg $K$ value of 3.1 and concentration of 580 μmol/g. This zeolite also contains another type of moderate acid site (lg $K$ = 5.3 and concentration = 130 μmol/g) which may be due to different coordination of the aluminum species (tetrahedral and octahedral) and their location in the framework: near framework and extra framework. Similar lg $K$ values of $R_1^-H^+$ are found in both H-Beta-25 and H-Beta-300 zeolites meaning that these acid sites are identical. On the other hand, the different lg $K$ values of $R_1^-H^+$ in the Beta zeolites and in the H-Ferrierite-20 zeolite are the sign of the fact that the aluminum atoms creating these two types of moderate acid sites, are in different frameworks. In their classical paper on the acid properties of silicates Schinler and Kamber gave lg $K$ value of 6.8 for silicate [31]. Iler reported additional lg $K$ values for silicate structures: 8.0–10.7 [32]. As can be seen in Table 2 similar values for the materials studied in this work were found and it can be concluded that these acid sites are due to the silicate structure in the materials and can be referred as the Lewis acid sites.

### 3.2. FTIR-pyridine method

The Brønsted and Lewis acid sites of the pristine H-Beta-25, H-Beta-300, H-Ferrierite-20 and Si-MCM-48 zeolites have been characterized by FTIR using pyridine as the test molecule (Table 3) [33,34]. The same method was also used to characterize the acid sites in the same zeolites after titration and those values are also included in Table 3. As can be seen in Table 3 the concentration of the acid sites determined by the FTIR-pyridine method is much lower in the same zeolite than when the potentiometric titration method is used (Table 2). Since the potentiometric titration was

**Table 2**
Protonation constants (lg $K$) and concentrations ($C$ μmol/g) of acid sites in the pristine zeolites determined by the Gran method.

| Acid sites | H-Beta-25 | | H-Beta-300 | | H-Ferrierite-20 | | Si-MCM-48 | |
|---|---|---|---|---|---|---|---|---|
| | lg $K$ | $C$ (μmol/g) | lg $K$ | $C$ (μmol/g) | lg $K$ | $C$ (μmol/g) | lg $K$ | $C$ (μmol/g) |
| $R_1^-H^+$ | 4.6 | 520 | 4.0 | 110 | 3.1 | 580 | | |
| $R_2^-H^+$ | 6.1 | 230 | 6.8 | 190 | 5.3 | 130 | | |
| $R_3^-H^+$ | 8.0 | 290 | 8.2 | 370 | 6.6 | 180 | 8.0 | 280 |
| $R_4^-H^+$ | | | | | 8.4 | 210 | | |
| Total | | 1040 | | 670 | | 1100 | | 280 |

**Table 3**
Concentrations of Brønsted acid sites (BAS) and Lewis acid sites (LAS) in the pristine and the titrated zeolites determined with FTIR-pyridine method.

| Zeolites | $C_{BAS}$ (μmol/g) | | | $C_{LAS}$ (μmol/g) | | | Total concentration (μmol/g) |
|---|---|---|---|---|---|---|---|
| | 250 °C | 350 °C | 450 °C | 250 °C | 350 °C | 450 °C | |
| Pristine H-Beta-25 [36] | 219 | 187 | 125 | 82 | 43 | 25 | 301 |
| Titrated H-Beta-25 | 0 | 0 | 0 | 55 | 11 | 9 | 55 |
| Pristine H-Beta-300 [36] | 54 | 49 | 23 | 28 | 9 | 4 | 82 |
| Titrated H-Beta-300 | 0 | 0 | 0 | 0 | 0 | 0 | 0 |
| Pristine H-Ferrierite-20 [37] | 349 | 339 | 275 | 8 | 4 | 2 | 357 |
| Titrated H-Ferrierite-20 | 0 | 0 | 0 | 0 | 0 | 0 | 0 |
| Pristine Si-MCM-48 | 0 | 0 | 0 | 12 | 3 | 0 | 12 |
| Titrated Si-MCM-48 | 0 | 0 | 0 | 3 | 0 | 0 | 3 |

done in an aqueous solution at 25 °C compared with the FTIR-pyridine method done in gaseous phase at elevated temperatures (250–450 °C), it is obvious that different values are obtained. In addition, some of the acid sites in the zeolite framework may not be accessible to the large pyridine molecules during the FTIR experiments while the small size of $OH^-$ ions makes it easy for them to penetrate in the small pores of zeolite.

The solid zeolite samples were collected after the potentiometric titration and their acidic properties were determined with the FTIR-pyridine method. The results are also shown in Table 3. During the titration Brønsted acid sites were neutralized and therefore the FTIR pyridine method did not show any of these sites in the studied zeolites. Lewis acid sites, however, were detected in the titrated H-Beta-25 but at lower concentrations than in the pristine zeolites. In the other titrated zeolites all the Lewis sites were neutralized.

### 3.3. X-ray powder diffraction method

The X-ray diffraction (XRD) patterns of the pristine zeolites as well as their titrated ones are shown in Fig. 5. As can be seen, all the titrated zeolites kept the main structural integrity intact compared with their pristine state, indicating that the base (NaOH) used for the titration was involved in the acid–base reaction with the acidic sites without destroying the main crystal structure of the zeolites. The interaction of $H_2O$ molecules with the Brønsted and Lewis acid sites has been studied in detail in Refs. [35,36].

### 3.4. Inductively Coupled Plasma Optical Emission Spectrometer (ICP-OES)

ICP-OES technique was used to measure the concentrations of aluminum and silicon in the studied zeolites. The results given in Table 4 include both the pristine zeolites and the same zeolites after the titrations. In the pristine zeolites the concentration of aluminum decreased in the order of H-Ferrierite-20 (1260 μmol/g) > H-Beta-25 (1000 μmol/g) > H-Beta-300 (150 μmol/g) > Si-MCM-48 (0 μmol/g), while the concentration of silicon decreased in the following order: Si-MCM-48 (14,400 μmol/g) > H-Beta-300 (14,200 μmol/g) > H-Beta-25 (13,200 μmol/g) > H-Ferrierite-20 (12,700 μmol/g). Comparing the results given in Tables 2 and 4, one can find that the concentration of aluminum correlates with

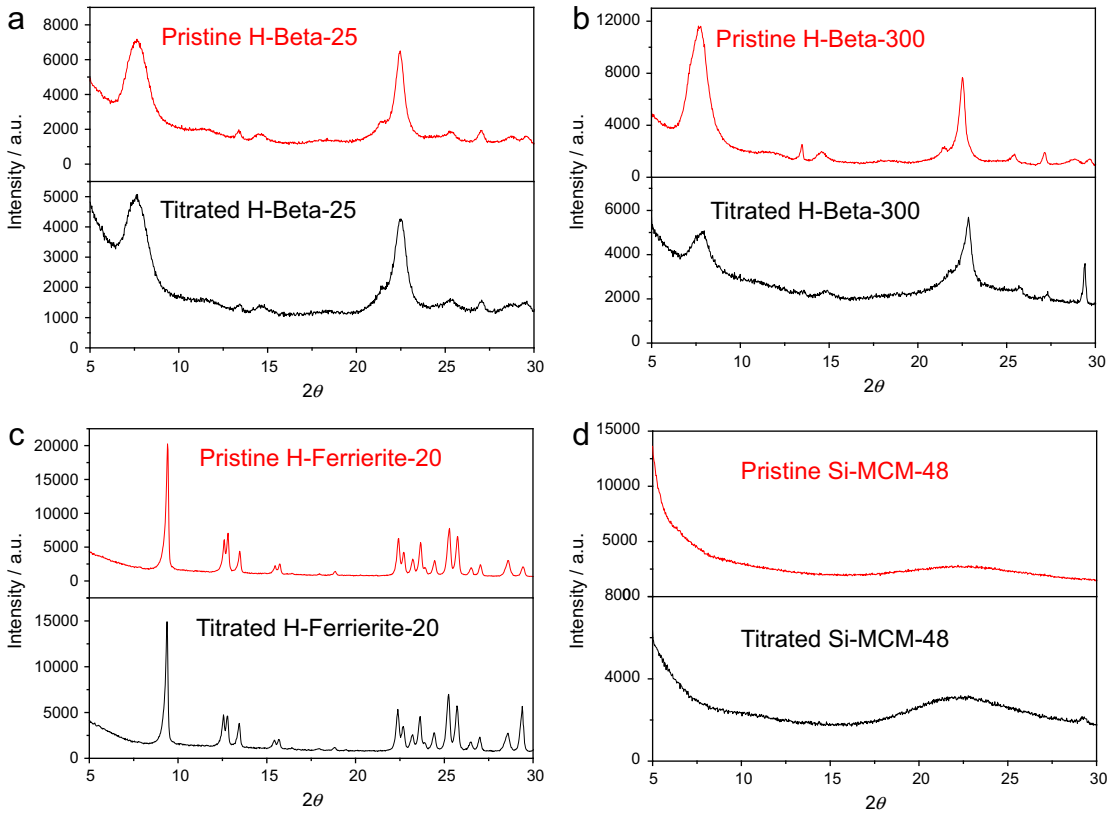


**Fig. 5.** XRD patterns of the pristine and titrated (a) H-Beta-25, (b) H-Beta-300, (c) H-Ferrierite-20 and (d) Si-MCM-48.

**Table 4**
The concentrations of silicon and aluminum in the pristine and titrated zeolites determined by ICP-OES, and the concentrations of the Brønsted acid sites (BAS) determined by the titration and the FTIR-pyridine methods.

| Zeolites | $C_{Si}$ (μmol/g) | $C_{Al}$ (μmol/g) | $SiO_2/Al_2O_3$ ratio | $C_{BAS}$ by titration (μmol/g) | $C_{BAS}$ by FTIR-pyridine (μmol/g) | $\frac{C_{BAS}\text{FTIR-pyridine}}{C_{BAS}\text{Titration}}$ (%) |
|---|---|---|---|---|---|---|
| Pristine H-Beta-25 | 13,200 | 1000 | 26 | 520 | 291 | 55 |
| Titrated H-Beta-25 | 12,200 | 860 | 28 | 0 | 0 | |
| Pristine H-Beta-300 | 14,200 | 150 | 200 | 110 | 54 | 49 |
| Titrated H-Beta-300 | 9300 | 110 | 170 | 0 | 0 | |
| Pristine H-Ferrierite-20 | 12,700 | 1260 | 20 | 710 | 349 | 49 |
| Titrated H-Ferrierite-20 | 11,000 | 1000 | 22 | 0 | 0 | |
| Pristine Si-MCM-48 | 14,400 | 0 | | 0 | 0 | |
| Titrated Si-MCM-48 | 13,000 | 0 | | | | |

the concentration of the Brønsted acid sites: high concentration of aluminum results in high concentration of the Brønsted acid sites. The molar ratios between $SiO_2$ and $Al_2O_3$ in the studied zeolites are also given in Table 4. The calculated value of the $SiO_2/Al_2O_3$ ratio 200 in H-Beta-300 may be due to the inaccuracy in the ICP-OES determination of the low concentration of aluminum in the sample.

Concentration of aluminum in the titrated zeolites follows the same order as in the pristine zeolites indicating that some aluminum was dissolved from all the zeolites. The H-Ferrierite-20 exhibited loss of 260 μmol/g of aluminum which can be attributed to the highest concentration of aluminum in its framework structure. However, the concentration of silicon in the titrated zeolites shows a different order than in the pristine zeolites: Si-MCM-48 (13,000 μmol/g) > H-Beta-25 (12,200 μmol/g) > H-Ferrierite-20 (11,000 μmol/g) > H-Beta-300 (9300 μmol/g). More silicon (4300 μmol/g) dissolved from H-Beta-300 implies that this zeolite may be unstable in the alkaline solution compared with the other three zeolites, but the framework of H-Beta-300 is still maintained after the titration (Fig. 5b).

Assuming that every Al atom in the tetrahedral framework creates a Brønsted acid site, the theoretical concentration of the acid sites in the studied zeolites is the same as the concentration of Al in them as given in Table 4. The experimentally determined total concentration of the Brønsted acid sites in one titrated zeolite can be calculated by combining the concentrations of the moderate acid sites which lg *K* values are <6.0 from Table 2. Those values are also included in Table 4. As can be seen the theoretical and the experimentally observed concentrations of the acid sites in zeolites differ from each other to some extent: 1000 μmol/g vs. 520 μmol/g (H-Beta-25), 150 μmol/g vs. 110 μmol/g (H-Beta-300), and 1260 μmol/g vs. 710 μmol/g (H-Ferrierite-20). This indicates that almost all of the aluminum in H-Beta-300 contributes to the Brønsted acid sites which are formed by aluminum in the framework, but approximately 48% of aluminum in H-Beta-25 and 44% of aluminum in H-Ferrierite-20 are located in the extra framework contributing to the Lewis acid sites. Concentrations of the Brønsted acid sites determined by the FTIR-pyridine method from Table 3 are also included in Table 4. In general, the proposed titration method gives results which are ca. 50–55% higher than

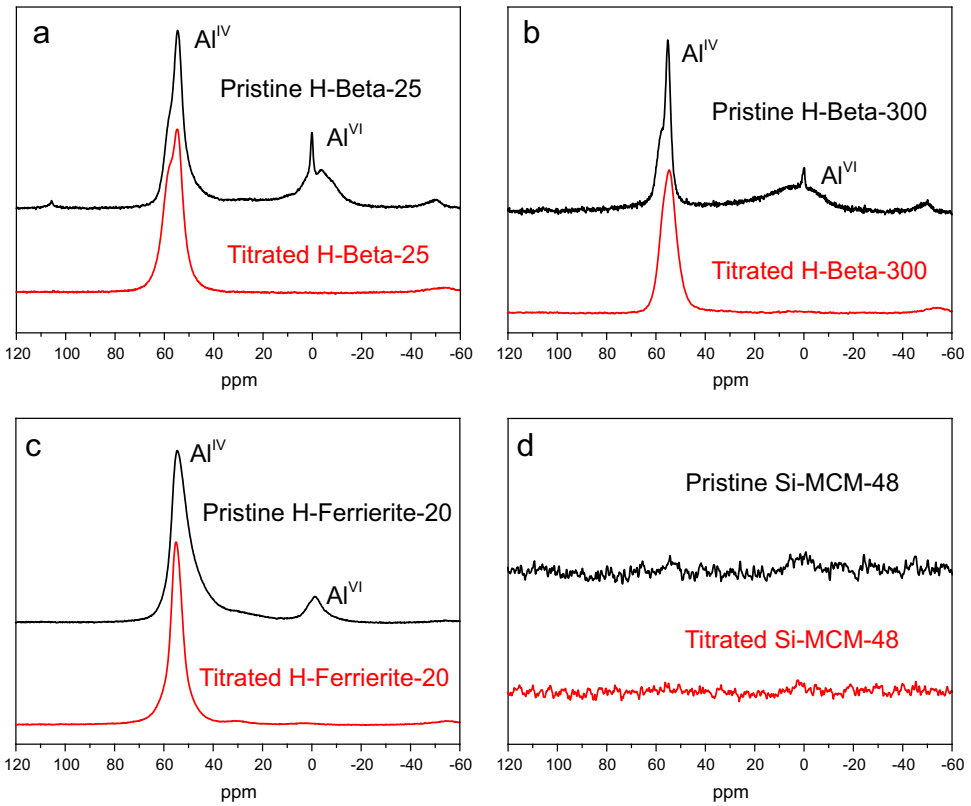


**Fig. 6.** $^{27}$Al MAS NMR spectra of the pristine and titrated zeolites (a) H-Beta-25, (b) H-Beta-300, (c) H-Ferrierite-20 and (d) Si-MCM-48.

**Table 5**
Framework aluminum contents in the pristine and titrated zeolites determined by MAS NMR method.

| Zeolites | Al in zeolites (%) | $Al^{IV}$ (a) in Al (%) | $Al^{IV}$ (b) in Al (%) | $Al^{IV}$ (c) in Al (%) | $Al^{V}$ in Al (%) | $Al^{VI}$ (a) in Al (%) | $Al^{VI}$ (b) in Al (%) |
|---|---|---|---|---|---|---|---|
| Pristine H-Beta-25 | 3.81 | 5 | 43 | 0 | 18 | 2 | 31 |
| Titrated H-Beta-25 | 3.27 | 42 | 58 | 0 | 0 | 0 | 0 |
| Pristine H-Beta-300 | 0.51 | 17 | 29 | 0 | 32 | 1 | 20 |
| Titrated H-Beta-300 | 0.42 | 27 | 73 | 0 | 0 | 0 | 0 |
| Pristine H-Ferrierite-20 | 4.09 | 29 | 31 | 27 | 0 | 12 | 0 |
| Titrated H-Ferrierite-20 | 3.77 | 97 | 0 | 0 | 1 | 2 | 0 |
| Pristine Si-MCM-48 | 0 | 0 | 0 | 0 | 0 | 0 | 0 |
| Titrated Si-MCM-48 | 0 | 0 | 0 | 0 | 0 | 0 | 0 |

the values obtained with the FTIR-pyridine method which can be explained by restricted accessibility of pyridine.

### 3.5. $^{27}Al$ MAS NMR spectroscopy

It is assumed that the concentrations of aluminum sites in aluminosilicate zeolites are related to the acidic property of these materials. Therefore, the coordination states of Al in both pristine and titrated zeolites have been characterized by $^{27}Al$ MAS NMR spectroscopy and the results are shown in Fig. 6 and Table 5. Two representative NMR peaks around 55 ($Al^{IV}$) and 0 ($Al^{VI}$) ppm are observed on the $^{27}Al$ NMR spectra of pristine H-Beta-25, H-Beta-300 and H-Ferrierite-20 in Fig. 6a–c. The resonance peak at 55 ppm with very strong intensity is attributed to the Al sites on the tetrahedral framework, and the peak at 0 ppm with very low intensity is assigned to the octahedral nonframework Al sites [37,38]. Only the $Al^{IV}$ peak can be found on the $^{27}Al$ NMR spectra of the titrated H-Beta-25, H-Beta-300 and H-Ferrierite-20, indicating that the tetrahedral Al sites are maintained but the octahedral Al sites are destroyed during the titration.

Table 5 shows that the contents of Al, $Al^{IV}$ and $Al^{VI}$ differ between the pristine and the titrated zeolites. For example, the Al content in H-Beta-25 decreased from 3.81% to 3.27% after the titration and the Al remained in the titrated zeolites is attributed completely to the tetrahedral $Al^{IV}$. A similar trend can also be observed in H-Beta-300 and H-Ferrierite-20 materials. In addition, most of Al in pristine H-Beta-25, H-Beta-300 and H-Ferrierite-20 catalysts is located in the tetrahedral framework. As expected, Al was not found in the pristine Si-MCM-48. No Brønsted acid sites were found in the titrated zeolites with FTIR-pyridine measurement, but the ICP-OES demonstrated that most of Al still remained in the structure and furthermore, these Al species are the tetrahedral framework $Al^{IV}$. In other words, the tetrahedral framework Al is much more stable than the octahedral nonframework Al in the alkaline environment [36].

Therefore, the presence of tetrahedral $Al^{IV}$ in the titrated zeolites can be attributed to strong interactions of Al species in the $[Al_2O_3–SiO_2]$ aluminosilicate framework. Differences in the percentage of $Al^{IV}$ in the titrated zeolites can be due to variations in the structures of zeolite i.e. Beta and Ferrierite, and also the amount of Al species present, i.e. variations in $SiO_2/Al_2O_3$ ratios. The absence of Brønsted acid sites as determined by FTIR-pyridine in the titrated zeolites contradicts the presence of tetrahedral $Al^{IV}$ species measured by $^{27}Al$ MAS NMR for the titrated zeolites. A plausible explanation for the absence of Brønsted acid sites as measured by FTIR-pyridine may be due to the decrease in the amount of $Al^{IV}$ left in the titrated zeolites. Another possible reason could be the inaccessibility of large pyridine molecule into the pores of the titrated zeolites due to some modification of the pores during titration. It is also noteworthy to mention that Lewis acid sites were determined by FTIR-pyridine for the titrated H-Beta-25. The presence of a substantial bulk amount of Al in the titrated zeolites measured by ICP-OES confirms strong interactions of Al species in the framework of $[Al_2O_3–SiO_2]$ and insignificant leaching of Al during the titration. However, these bulk aluminum species contain both the tetrahedral framework ($Al^{IV}$) and the octahedral framework ($Al^{V}$ and $Al^{VI}$). Structural integrity of the titrated zeolites was confirmed by the XRD patterns. All the titrated zeolites exhibited similar XRD patterns to that of the pristine ones; hence, absence of Brønsted acid sites measured by FTIR-pyridine in the titrated zeolites cannot be attributed to the distortion of zeolites structure.

## 4. Conclusions

Potentiometric titration of zeolites with a strong base in aqueous solutions at ambient temperatures is proved to be a useful method to characterize the acid sites in microporous and mesoporous materials. The Brønsted and Lewis acid sites can be distinguished with this method. Concentrations of the acid sites in the zeolite frameworks, determined by the potentiometric titration, are much higher than when determined with the FTIR-pyridine method. The higher concentrations observed are attributed to the small size of the $OH^-$ ions used in the potentiometric titration. These small ions can penetrate deep in the zeolite channels and therefore the acid sites even in those channels can be determined. The FTIR-pyridine method is performed in the gas phase and has to be done at elevated temperatures (350–450 °C) with large pyridine molecules which may not access all the acid sites located inside the pores. It was also demonstrated by the FTIR-pyridine method that the acid sites, especially the Brønsted sites, were neutralized during the titration.

Although some aluminum and silicon were found to leach away from the studied zeolite after titration, the framework of the titrated zeolites was still maintained. Al species remained in the titrated zeolites are attributed to the tetrahedral framework $Al^{IV}$. In other words, the tetrahedral framework Al is much more stable than the octahedral nonframework Al in the alkaline environment.

Thus, the potentiometric titration is a reliable and suitable method for characterizing the acidic properties of zeolites which are used in the aqueous phase catalytic reactions at ambient temperature.

## Acknowledgment

This work is part of the activities of Åbo Akademi *Johan Gadolin* Process Chemistry Centre (ÅA-PCC), Finland.

## Appendix A. Supplementary material

Supplementary data associated with this article can be found, in the online version, at http://dx.doi.org/10.1016/j.jcat.2015.12.010.

## References


[1] L.B. McCusker, C. Baerlocher, in: J. Cejka, H. Van Bekkum, A. Corma, F. Schüth (Eds.), Introduction to Zeolite Science and Practice, Elsevier B.V, Amsterdam, 2007.
[2] J.A. Lercher, A. Jentys, in: F. Schüth, K.S.W. Sing, J. Weitkamp (Eds.), Handbook of Porous Solids, Wiley-VCH, Weinheim, 2002, p. 1097.
[3] K.H. Lee, J. Anal. Appl. Pyrolysis 94 (2012) 209–214.
[4] A.K. Aboul-Gheit, A.E. Awadallah, J. Nat. Gas Chem. 18 (2009) 71–77.
[5] S.B. Wang, Y.L. Peng, Chem. Eng. J. 156 (2010) 11–24.
[6] K. Ramesh, D.D. Reddy, Adv. Agron. 113 (2011) 219–241.
[7] T.Y. Wang, S.H. Yang, K. Sun, X.F. Fang, Ceram. Int. 37 (2) (2011) 621–626.
[8] Y.A. Mustafa, M.J. Zaiter, J. Hazard. Mater. 196 (2011) 228–233.
[9] A. Auroux, Mol. Sieves 6 (2008) 45–152.
[10] N. Batalha, S. Morisset, L. Pinard, I. Maupin, J.L. Lemberton, F. Lemos, Y. Pouilloux, Microporous Mesoporous Mater. 166 (2013) 101–166.
[11] F. Jin, Y.D. Li, Catal. Today 1–2 (2009) 101–107.
[12] L. Rodriguez-Gonzalez, F. Hermes, M. Bertmer, E. Rodriguez-Castellon, A. Jimenez-Lopez, U. Simon, Appl. Catal. A 328 (2007) 174–182.
[13] M. Käldström, N. Kumar, D.Yu. Murzin, Catal. Today 167 (2011) 91–93.
[14] M. Käldstöm, N. Kumar, T. Salmi, D.Yu. Murzin, Cellul. Chem. Technol. 44 (2010) 203–209.
[15] H.A. Benesi, J. Am. Chem. Soc. 78 (21) (1956) 5490–5494.
[16] P. Janos, S. Krizenecka, L. Madronova, React. Funct. Polym. 68 (2008) 242–247.
[17] A.E. Hirschler, A. Schneider, J. Chem. Eng. Data 6 (2) (1961) 313–318.
[18] A. Streitwieser, Y.J. Kim, J. Am. Chem. Soc. 122 (2000) 11783–11786.
[19] E.G. Derouane, J.C. Védrine, R.R. Pinto, P.M. Borges, L. Costa, M.A.N.D.A. Lemos, F. Lemos, R.R. Ribeiro, Cat. Rev. Sci. Eng. 55 (2013) 454–515.
[20] A. Jentys, J.A. Lercher, in: H. Van Bekkum, E.M. Flanigen, P.A. Jacobs, J.C. Jansen (Eds.), Studies in Surface Science and Catalysis-Introduction to Zeolite Science and Practice, Elsevier BV, Amsterdam, 2001, p. 345.
[21] <http://www.iza-structure.org/databases/> 2015.
[22] A.D. Roberts, X. Li, H.F. Zhang, Chem. Soc. Rev. 43 (2014) 4341–4356.
[23] A. Aho, N. Kumar, K. Eränen, T. Salmi, M. Hupa, D.Yu. Murzin, Fuel 87 (2008) 2493–2501.
[24] M. Kangas, N. Kumar, E. Harlin, T. Salmi, D.Y. Murzin, Ind. Eng. Chem. Res. 47 (2008) 5402–5412.
[25] M. Käldström, N. Kumar, T. Heikkilä, M. Tiitta, T. Salmi, D.Yu. Murzin, ChemCatChem 2 (2010) 539–546.
[26] P. Sørensen, Kem. Maanedsblad 32 (1951) 73.
[27] G. Gran, Analyst 77 (1952) 661–671.
[28] F. Ingman, E. Still, Talanta 13 (1966) 1431–1442.
[29] A. Ivaska, E. Wänninen, Anal. Lett. 6 (1973) 961–967.
[30] D. Coster, A.L. Blumenfeld, J. Fripiat, J. Phys. Chem. 98 (1994) 6201–6211.
[31] P.W. Schinler, H.R. Kamber, Helv. Chim. Acta 51 (1968) 1781–1786.
[32] R.K. Iler, in: Anonymous (Ed.), The Chemistry of Silica, Johan Wiley and Sons, New York, 1979, pp. 180–183.
[33] A. Aho, N. Kumar, K. Eränen, T. Salmi, M. Hupa, D.Yu. Murzin, Trans. IChemE, Part B 85 (B5) (2007) 473–480.
[34] A. Aho, N. Kumar, K. Eränen, M. Ziolek, P. Decyk, A.V. Lashkul, T. Salmi, B. Holmbom, M. Hupa, D.Yu. Murzin, Fuel 89 (2010) 1992–2000.
[35] V. Bolis, C. Busco, J. Phys. Chem. 110 (2006) 14849–14859.
[36] D.H. Olson, W.O. Haag, W.S. Borghard, Microporous Mesoporous Mater. 35–36 (2000) 435–446.
[37] R. Hajjar, Y. Millot, P.P. Man, M. Che, S. Dzwigaj, J. Phys. Chem. C 112 (2008) 20167–20175.
[38] D.P.B. Peixoto, S.M. Cabral de Menezes, M.I. Pais da Silva, Mater. Lett. 57 (2003) 3933–3942.